
Real-Time Anomaly Detection System for Data Quality Monitoring in the CMS ECAL using Autoencoders

Abhirami Harilal, on behalf of the CMS Collaboration

Department of Physics
Carnegie Mellon University
Pittsburgh, PA, USA
aharilal@andrew.cmu.edu

Abstract

Large-scale experiments such as the CMS detector, a general-purpose apparatus that records high-energy collisions at the CERN LHC, involve complex detector components and operate under changing conditions, making continuous monitoring essential to ensure physics-quality data. In the CMS electromagnetic calorimeter, traditional cut-based data quality monitoring (DQM) addresses known issues but has limited ability to detect rare or unforeseen anomalies. We present a semi-supervised anomaly detection framework based on autoencoders, developed for and deployed in the CMS online DQM workflow during the LHC Run 3 (2022–2026). The method improves performance by incorporating both the temporal evolution of anomalies and spatial variations of the detector response. Deployment results from Run 3 are presented, showing that the system detected issues missed by the existing monitoring and provided early indications of degrading components. The framework enables real-time anomaly detection with a very low false-alarm rate, representing one of the first operational uses of deep learning for DQM in high-energy physics and offering a generalizable approach for other scientific experiments.

1 Introduction

Modern high-energy physics experiments employ highly complex detectors that must deliver physics-quality data under harsh and continuously changing conditions, where effects such as radiation damage and hardware degradation can impact performance. Maintaining data quality is therefore essential for enabling precision measurements and discoveries. The Compact Muon Solenoid (CMS) detector [1, 2] at the CERN Large Hadron Collider (LHC) exemplifies this challenge: its electromagnetic calorimeter (ECAL) measures the energy of electrons and photons with high precision, a capability that was central to the discovery of the Higgs boson [3, 4] and remains vital for ongoing efforts in both precision physics and new physics searches.

To safeguard performance, CMS operates a data quality monitoring (DQM) system [5]. The traditional online DQM workflow relies on pre-defined metrics and distributions filled in real time from detector data, which are then continuously inspected by human *shifters*. This system applies specific rules tailored to each detector part and geometry and is effective for identifying recurring or well-understood failure modes, but has limited sensitivity to rare, unforeseen, or gradually evolving anomalies. Machine learning (ML) offers an attractive alternative, by learning typical detector behavior directly from data and automatically flagging deviations that may not be captured by hand-crafted rules or thresholds.

We develop and deploy a semi-supervised autoencoder (AE)-based anomaly detection system for CMS ECAL, designed to complement traditional DQM by identifying subtle or rare issues it may

miss. The method, incorporating spatial and temporal corrections, has been integrated into CMS online operations during LHC Run 3 and published in Ref. [6].

2 Data Quality Monitoring in the CMS ECAL

The CMS ECAL is a high-resolution calorimeter that measures the energy, timing, and position of photons, electrons, and the electromagnetic component of jets. It is built from nearly 76,000 scintillating lead tungstate crystals, arranged in a cylindrical barrel section (EB) and two endcaps (EE+ and EE−). The crystals are segmented in pseudorapidity (η) and azimuthal angle (ϕ), providing a natural 2D geometry that is commonly used to visualize detector components.

The performance of ECAL is continuously tracked through a dedicated DQM system which relies on histograms that are automatically filled with detector data during operation. Two main types are used: Occupancy-style histograms, as shown in Figure 2 (top left) which display raw detector quantities such as energy deposits or noise values, and Quality-style histograms as shown in Figure 2 (bottom left) which apply predefined thresholds to the occupancy-style distributions. Quality histograms are presented as color-coded maps – green for *good*, red for *bad*, brown for *known issues* and yellow for *no data* – that provide an immediate visual snapshot of the detector status. These maps are often displayed at the “readout tower” level (henceforth referred to as a tower), each representing a 5×5 group of crystals. During LHC operation, CMS records data in hour-long *runs*, divided into ~ 23 second intervals called *lumisections* (LS). DQM histograms are updated per LS and accumulated over runs, allowing both short-term and long-term detector monitoring.

At higher luminosities and under more intense radiation conditions, it is not feasible to predict all potential failure modes in a detector as complex as the ECAL. The existing DQM alarms rely on hard-coded rules tied to detector geometry and often produce high false-positive rates. These limitations motivate automated, ML-based approaches to anomaly detection.

3 Autoencoder-based Anomaly Detection System

The anomaly detection framework is based on a convolutional AE with residual connections following the ResNet architecture [7] trained in a semi-supervised setting. Separate models are trained for the EB, EE+, and EE- regions to account for geometric and response differences, using occupancy maps from individual LSs in CMS Run 2 data (2018). The training dataset is composed exclusively of certified good data, allowing the network to learn typical detector response patterns and identify deviations as potential anomalies. The encoder compresses the input image into a compact latent representation using progressive convolutional layers, while the decoder reconstructs it back to the original form. The similarity between input and output is quantified using a reconstruction loss (\mathcal{L}) computed as the Mean Squared Error (MSE) between input (x) and reconstruction (x') as $\mathcal{L}(x, x') = ||(x - x')||^2$.

The network architecture, illustrated in Figure 1, follows an encoder–decoder design built from sequential residual blocks (ResBlocks). Each ResBlock comprises two 3×3 convolutional layers with an intermediate ReLU activation [8] and an identity skip connection. The encoder takes as input occupancy images of size 36×72 for the EB and 22×22 for the EE, performing convolution and max-pooling operations to reduce spatial dimensions while increasing feature depth. The resulting feature maps are passed through stacked ResBlocks, followed by a global max-pooling layer that produces a compact latent representation. The decoder mirrors this structure with upsampling layers that reconstruct the input map from the encoded space.

During inference, the AE reconstructs nominal inputs with low loss, while anomalous regions yield higher local loss, forming the basis of the anomaly detection strategy, as illustrated in Figure 2 for the endcaps. The AE takes the input occupancy image (top left) and outputs a reconstructed image (top right). A tower-wise MSE is then computed to produce a 2D loss map, where anomalous regions appear with elevated loss values (bottom right). After applying the post-processing steps described in Sec. 3.1, a threshold is derived from the anomalous loss values that can efficiently detect 99% of the anomalies. This threshold is applied to the post-processed loss map to generate a quality plot (bottom left), marking anomalous towers in red and good towers in green.

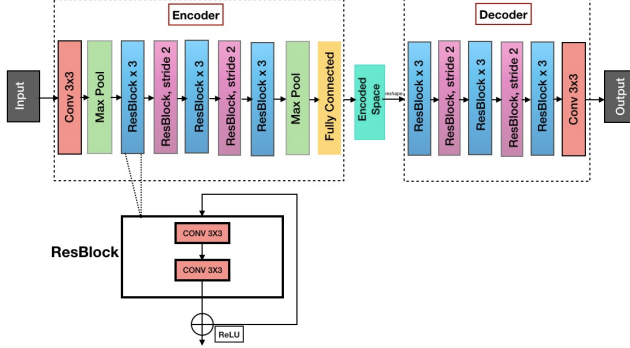


Figure 1: AE architecture showing the encoder and decoder networks, with the ResBlock structure displayed.

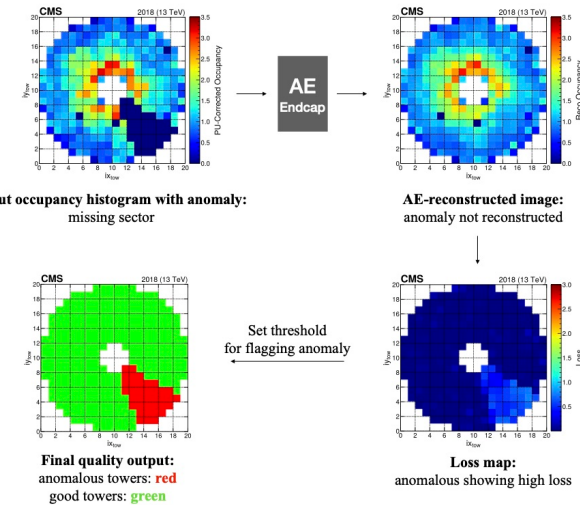


Figure 2: Illustration of the AE-based anomaly detection strategy.

3.1 Post processing : Spatial and Time Corrections

In ECAL, regions closer to the beam pipe (high $|\eta|$) naturally exhibit higher particle occupancy than those at lower $|\eta|$. This leads to a bias in the loss maps: anomalies can appear more severe at high $|\eta|$ even when all affected towers are equally anomalous. Figure 3 shows this effect for a missing supermodule (group of 68 towers) in the EB. The input occupancy map (a) shows the missing region, while the AE-reconstructed output (b) fails to reproduce the anomaly. The resulting uncorrected loss map (c) highlights higher losses at large $|\eta|$ due to occupancy differences. A spatial response correction is applied by normalizing the loss map with the average occupancy from good data, yielding a uniform anomaly region as shown in (d).

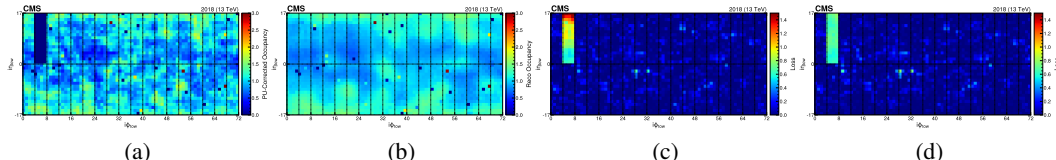


Figure 3: (a) Input occupancy map with a missing supermodule in the barrel. (b) AE-reconstructed output. (c) Resulting loss map showing higher loss at high $|\eta|$ due to differences in the detector response. (d) Uniform loss map after the spatial correction is applied.

Real detector anomalies tend to persist with time across consecutive LSs, whereas statistical fluctuations average out. To exploit this, a “time correction” is applied in which spatially corrected loss maps from three consecutive LSs are multiplied at the tower level. This enhances the persistent structures while suppressing random noise. The result is a significant reduction in false positives and an overall improvement in anomaly detection performance.

4 Results

4.1 Validation with Fake Anomalies

The ML-based DQM system is designed to balance two objectives: reliably detecting anomalies while minimizing false alarms. Anomalies are identified by applying a threshold derived from a validation sample with injected “fake” anomalies. This threshold is set on the post-processed loss map such that 99% of anomalous towers have loss values above it. To evaluate performance, we use the False Discovery Rate (FDR), defined as the fraction of good towers incorrectly flagged as anomalous out of all towers labeled as anomalous at the 99% anomaly detection efficiency operating point. Lower FDR corresponds to fewer false alarms during data taking.

The AE-based anomaly detection is compared against a baseline following the traditional cut-based DQM approach for the EB. A baseline loss is defined for each tower at a given (ϕ, η) position as the absolute deviation of its occupancy from the mean occupancy of all towers within the same η -ring, which mirrors the standard ECAL DQM logic. A similar baseline loss is not computed for the endcaps, as steep occupancy gradients within η -rings make such a metric unreliable for anomaly detection in those regions.

Table 1 summarizes the measured FDR for different artificial anomaly types across ECAL regions. At the same 99% detection point, the AE consistently outperforms the cut-based baseline, which remains less effective even after applying equivalent corrections. Hot towers were the easiest to detect, while zero-occupancy towers were more challenging. The observed trends follow detector-specific effects: the spatial correction provides the largest improvement in the endcaps, where occupancy gradients across $|\eta|$ are most pronounced. For hot-tower anomalies, however, the FDR increases slightly after the spatial correction, as this flattens local gradients that help isolate high-occupancy towers. This effect is mitigated by the subsequent time correction, which significantly improves the FDRs and yields the best overall performance. Across all cases, final FDR values reached the 10^{-2} – 10^{-4} range, with most remaining false positives corresponding to actual anomalous towers that were not severe enough to be excluded from the certified good data.

Table 1: FDR (in %) at 99% anomaly detection threshold for fake anomaly validation across ECAL regions.

	EB			EE+			EE-		
	Missing SM	Zero Occ. Tower	Hot Tower	Missing Sector	Zero Occ. Tower	Hot Tower	Missing Sector	Zero Occ. Tower	Hot Tower
Baseline (no corr.)	14	90	5.2	—	—	—	—	—	—
Baseline + time corr.	5.9	80	< 0.01	—	—	—	—	—	—
AE (no corr.)	3.6	51	2.8	29	86	< 0.01	28	86	< 0.01
AE + spatial corr.	3.1	49	2.9	1.8	11	0.02	2.2	14	0.04
AE + spatial & time corr.	0.13	4.1	< 0.01	0.06	1.4	< 0.1	0.18	4.4	< 0.1

4.2 MLDQM - Deployment and performance on real anomalies

Prior to deployment, the method was validated on real detector issues observed in 2018 and 2022 runs, confirming its ability to detect localized anomalies. The AE-based anomaly detection system, named MLDQM, was integrated into the CMS ECAL online DQM workflow at the start of Run 3. The trained PyTorch [9] models were exported to ONNX [10] and deployed within the CMS software framework using ONNX Runtime [11]. The model inference runs within the ECAL online DQM sequence, sharing the same event streams as standard monitoring, and introduces negligible latency (< 1 s per LS). During deployment, the inference achieves near real-time performance, with the first quality plot produced after \sim 3 minutes (9 LS) and subsequent updates every LS. The system produces quality maps using a single threshold for each ECAL subdetector and has successfully

flagged real issues during operation. Flagged towers from each LS are stored for offline aggregation across runs, supporting expert cross-checks with other DQM observables and enabling long-term monitoring of recurring detector issues. The deployed model has remained stable throughout Run 3 without retraining, with performance maintained by periodically updating the reference occupancy maps using the latest certified good data.

As an illustration, Fig. 4(a) shows a quality plot produced by the deployed MLDQM for the EB. Two anomalous towers are marked with red circles in supermodules EB+06 and EB-06. In the corresponding occupancy histogram in Fig. 4(b), both towers exhibit zero occupancy, confirming that the deployed system accurately flags real anomalies. Other zero occupancy towers correspond to known persistent issues present in the training dataset, and are therefore ignored by the AE.

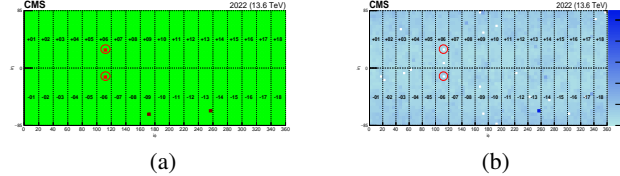


Figure 4: Example of real anomaly detection during the 2022 deployment. (a) MLDQM quality map in the online ECAL DQM showing two flagged towers in red circles. (b) Corresponding occupancy plot for the same LS, where both towers show zero occupancy, confirming accurate identification of real detector issues.

The MLDQM system was also observed to flag new towers with transient anomalous behavior that were missed by the existing DQM. Fig. 5(a) shows the MLDQM quality plot accumulated over 9 LSs from a 2022 run with two flagged bad towers in red circles in EB+08. Fig. 5(b) shows the occupancy over the same full run where Tower 1 shows persistently low occupancy, while Tower 2 is only faintly visible, indicating intermittent zero occupancy. This feature is also observed in Fig. 5(c), where the average occupancy across multiple runs shows Tower 2 with reduced occupancy, confirming it is not a random single-event anomaly. These observations motivated tracking the frequency with which specific towers are flagged as anomalous, recorded per LS and accumulated across runs, enabling long-term monitoring and proactive identification of degrading channels – a capability previously absent in the ECAL DQM system.

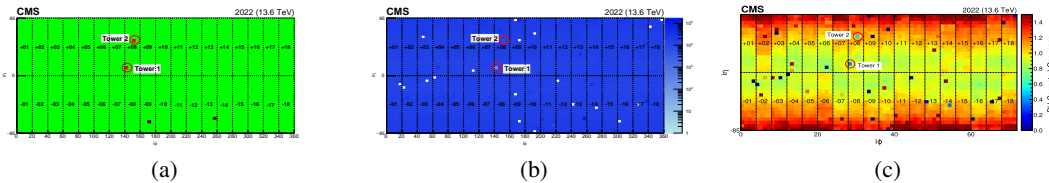


Figure 5: Example of transient anomalies detected in 2022 data. (a) Quality map over 9 LSs showing two flagged towers in red circles. (b) Full-run occupancy map showing Tower 1 with persistently low occupancy and Tower 2 intermittently affected. (c) Average occupancy across multiple runs showing recurring low occupancy of Tower 2.

5 Summary

We developed and deployed a semi-supervised autoencoder-based anomaly detection system for the CMS ECAL, integrated into the online DQM workflow since Run 3. Correction strategies that account for spatial response variations and the time-dependent nature of anomalies, yield order-of-magnitude improvements in performance. A single optimized threshold per detector region enables robust tagging at tower-level granularity. This system enhances the traditional DQM by autonomously identifying anomalous detector behavior and demonstrates a scalable deep learning-based framework applicable to other experiments.

References

- [1] CMS Collaboration. The CMS experiment at the CERN LHC. *JINST*, 3:S08004, 2008. doi: 10.1088/1748-0221/3/08/S08004.
- [2] CMS Collaboration. Development of the CMS detector for the CERN LHC Run 3. *JINST*, 19: P05064, 2024. doi: 10.1088/1748-0221/19/05/P05064.
- [3] ATLAS Collaboration. Observation of a new particle in the search for the Standard Model Higgs boson with the ATLAS detector at the LHC. *Phys. Lett. B*, 716:1–29, 2012. doi: 10.1016/j.physletb.2012.08.020.
- [4] CMS Collaboration. Observation of a New Boson at a Mass of 125 GeV with the CMS Experiment at the LHC. *Phys. Lett. B*, 716:30–61, 2012. doi: 10.1016/j.physletb.2012.08.021.
- [5] Virginia Azzolini, Broen van Besien, Dmitrijus Bugelskis, Tomas Hreus, Kaori Maeshima, Javier Fernandez Menendez, Antanas Norkus, James Fraser Patrick, Marco Rovere, and Marcel Andre Schneider. The Data Quality Monitoring software for the CMS experiment at the LHC: past, present and future. *EPJ Web Conf.*, 214:02003, 2019. doi: 10.1051/epjconf/201921402003.
- [6] The CMS ECAL Collaboration. Autoencoder-based anomaly detection system for online data quality monitoring of the cms electromagnetic calorimeter. *Computing and Software for Big Science*, 8(1), June 2024. ISSN 2510-2044. doi: 10.1007/s41781-024-00118-z. URL <http://dx.doi.org/10.1007/s41781-024-00118-z>.
- [7] Kaiming He, Xiangyu Zhang, Shaoqing Ren, and Jian Sun. Deep Residual Learning for Image Recognition. 12 2015. doi: 10.1109/CVPR.2016.90.
- [8] Vinod Nair and Geoffrey E. Hinton. Rectified linear units improve restricted boltzmann machines. In *Proceedings of the 27th International Conference on International Conference on Machine Learning*, ICML’10, pages 807–814, USA, 2010. Omnipress. ISBN 978-1-60558-907-7. URL <http://dl.acm.org/citation.cfm?id=3104322.3104425>.
- [9] Adam Paszke, Sam Gross, Francisco Massa, Adam Lerer, James Bradbury, Gregory Chanan, Trevor Killeen, Zeming Lin, Natalia Gimelshein, Luca Antiga, Alban Desmaison, Andreas Kopf, Edward Yang, Zachary DeVito, Martin Raison, Alykhan Tejani, Sasank Chilamkurthy, Benoit Steiner, Lu Fang, Junjie Bai, and Soumith Chintala. Pytorch: An imperative style, high-performance deep learning library. In H. Wallach, H. Larochelle, A. Beygelzimer, F. d’Alché-Buc, E. Fox, and R. Garnett, editors, *Advances in Neural Information Processing Systems 32*, pages 8024–8035. Curran Associates, Inc., 2019. URL <http://papers.neurips.cc/paper/9015-pytorch-an-imperative-style-high-performance-deep-learning-library.pdf>.
- [10] Junjie Bai, Fang Lu, Ke Zhang, et al. Onnx: Open neural network exchange. <https://github.com/onnx/onnx>, 2019.
- [11] ONNX Runtime developers. Onnx runtime. <https://onnxruntime.ai/>, 2021.